How to cite: *Angew. Chem. Int. Ed.* **2025**, *64*, e202414908
doi.org/10.1002/anie.202414908

Nanoclusters for CO_2 Reduction | Hot Paper

Encapsulation of an Au_{25} Nanocluster inside a Porphyrin Nanoring Enhances Singlet Oxygen Generation and Photo-Electrocatalytic CO_2 Reduction

Abolfazl Ziarati[+], Henrik Gotfredsen[+], Arnulf Rosspeintner, Jiangtao Zhao, Harry L. Anderson,* and Thomas Bürgi**

Abstract: The synthesis of molecular host–guest complexes with enhanced performance, relative to those of their components, is a central theme in supramolecular chemistry. Here we explore a host-guest system consisting of an atomically precise gold nanocluster bound inside a zinc porphyrin nanoring. UV/Vis absorption and fluorescence titrations with different sized nanorings revealed strong binding between a pyridinethiol-coated Au_{25} nanocluster and a nanoring consisting of six zinc porphyrin units, and complexation is confirmed by mass spectrometry. Formation of this assembly enhances the stability of the gold nanocluster. The host-guest complex also exhibits remarkable activity and selectivity for photochemical CO_2 to CO conversion and singlet oxygen generation.

Introduction

Ligand-protected metal nanoclusters have unique physical and chemical properties owing to their intermediate size between individual atoms and bulk materials.[1] Atomically precise gold nanoclusters have rapidly emerged as nanomaterials with size-dependent molecular properties for a broad spectrum of applications, especially in catalysis and sustainable energy.[2] Au nanoclusters exhibit remarkable photocatalytic activity,[3] offering a promising avenue for generating singlet oxygen[4] – a species with applications in various fields, including photodynamic therapy and environmental remediation.[5] Au nanoclusters also show potential for converting CO_2 into valuable products during illumination,[6] contributing to efforts in mitigating climate change and presenting an innovative approach to sustainable energy conversion. However, the tight ligand capping of Au nanoclusters hinders adsorption of reactants, reducing their catalytic activity.[6b] Moreover, Au nanoclusters typically suffer from poor stability due to aggregation and coalescence, especially during photocatalytic reactions.[7] Here we explore supramolecular encapsulation of the Au nanoclusters as a strategy for enhancing their photochemistry and hindering aggregation. π-Conjugated cyclic porphyrin oligomers (also known as "porphyrin nanorings") are promising hosts, due to their photophysical properties,[8] binding behavior[9] and structural/size diversity.[10] Porphyrin nanorings have been synthesized with diameters of up to more than 20 nm, making them large enough to encapsulate a wide range of Au nanoclusters. Furthermore, Au nanoclusters have previously been synthesized with pyridine-functionalized thiol coats,[11] which makes them ideal for coordinating inside the cavities of zinc porphyrin nanorings. These nanorings exhibit high charge mobility and excited state delocalization,[8,12] which could facilitate the transfer of photogenerated electrons towards the active site and thus promote catalytic activity.

$Au_{25}(SR)_{18}$ complexes are among the most well-studied molecular gold nanoclusters.[13] They consist of a central gold atom surrounded by an icosahedral Au_{12} shell, with 12 more Au atoms capping faces of the icosahedron, protected by a coat of 18 thiolate ligands.[14] The anionic clusters $Au_{25}(SR)_{18}^-$ have closed-shell electronic configurations, whereas neutral $Au_{25}(SR)_{18}^0$ clusters have unpaired electrons. Here we report the host–guest complexation between butadiyne-linked porphyrin nanorings (***c*-P*N***, $N=6$, 8, 10) and an Au_{25} nanocluster functionalized with 18 flexible 4-pyridylethylthiolate ligands: the anionic nanocluster $\mathbf{Au_{25}PyET_{18}^-}$ (Figures 1 and S1–S4; PyET = 4-pyridylethylthiolate). The application of these encapsulated nanoclusters is demonstrated in the case of ***c*-P6•Au$_{25}$PyET$_{18}^-$** for both singlet oxygen generation and photo-coupled electrocatalytic CO_2 reduction. In both cases, the complex, ***c*-P6•Au$_{25}$PyET$_{18}^-$**, performs better than either the pristine $\mathbf{Au_{25}PyET_{18}^-}$ nanocluster or ***c*-P6** alone.

[*] Dr. A. Ziarati,[+] Dr. A. Rosspeintner, J. Zhao, Prof. T. Bürgi
Department of Physical Chemistry, University of Geneva, 30 Quai Ernest-Ansermet,1211 Geneva 4 (Switzerland)
E-mail: Abolfazl.Ziarati@unige.ch
Thomas.Buergi@unige.ch
Dr. H. Gotfredsen,[+] Prof. H. L. Anderson
Department of Chemistry, University of Oxford, Chemistry Research Laboratory, Oxford OX1 3TA (UK)
E-mail: Harry.Anderson@chem.ox.ac.uk
[+] These authors contributed equally to this work.

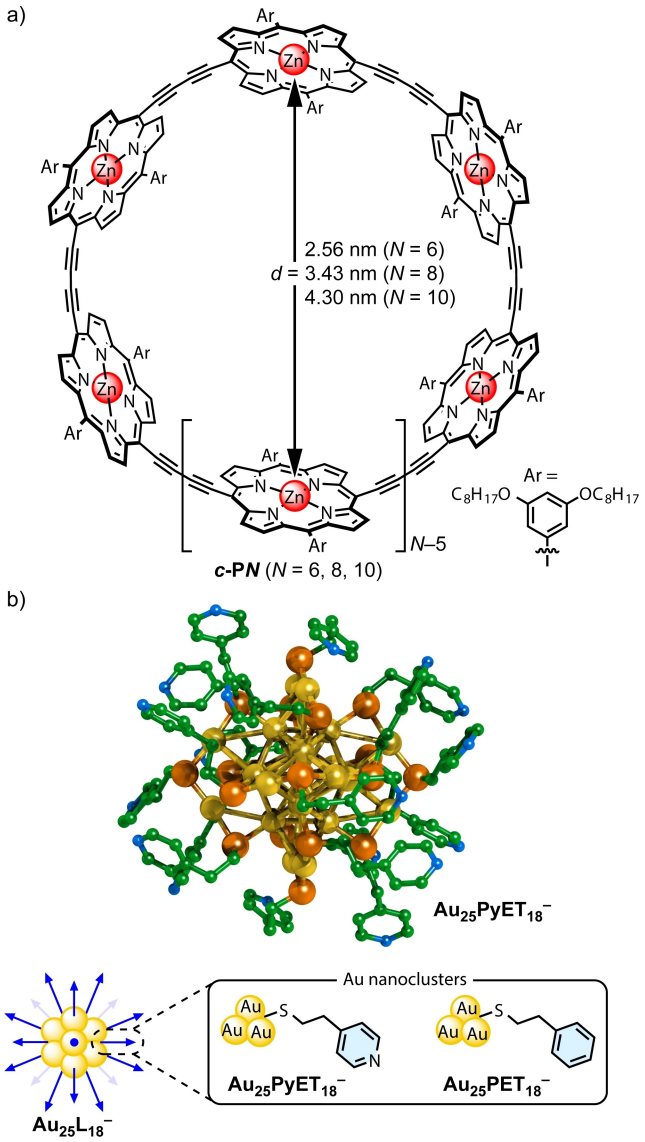

Figure 1. Porphyrin nanorings (a) and gold nanoclusters (b) included in this work. PyET = 4-pyridylethylthiolate, PET = 4-phenylethylthiolate. The model of $\mathbf{Au_{25}PyET_{18}^-}$ is derived from the crystal structure of $\mathbf{Au_{25}PyET_{18}Na}$.[11]

Results and Discussion

Design of the host-guest complex

We started this project by modelling different nanocluster-nanoring combinations to identify a good match, in terms of size and shape, between a pyridyl decorated gold nanocluster (the guest) and a porphyrin nanoring (the host). We realized that the Au_{25} nanocluster with 4-pyridylethyl thiol surface ligands ($\mathbf{Au_{25}PyET_{18}^-}$) might be a suitable guest for ***c*-P6**. The X-ray crystal structure of $\mathbf{Au_{25}PyET_{18}^-}$ shows that the distances of the 4-pyridyl nitrogen binding sites from the center of the cluster are in the range 8.71–10.77 Å (mean 9.85 Å; standard deviation 0.77 Å).[11] The ideal diameter of a template for binding ***c*-P6** can be calculated from the Zn···Zn diameter of the empty nanoring ($d_{\mathbf{Zn\text{-}Zn}} = 2.56$ nm, from DFT calculations[15]), taking account of the N-(pyridine)–Zn(porphyrin) bond length (2.16 Å) and the distance by which the zinc atom moves out of the plane of the porphyrin when it becomes 5-coordinate (0.37 Å).[16] Thus the ideal N···N template diameter for binding ***c*-P6** is $d_{\text{template}} = d_{\mathbf{Zn\text{-}Zn}} - 2\times(0.216+0.037) = 2.05$ nm. The crystallographic N···N diameter of $\mathbf{Au_{25}PyET_{18}^-}$ is 1.97 ± 0.15 nm, which indicates a good size-match for ***c*-P6**. However, the nitrogen binding sites around $\mathbf{Au_{25}PyET_{18}^-}$ are not in a regular hexagonal arrangement. The ligand surface geometry of an $Au_{25}(SR)_{18}$ nanocluster implies that an 8-porphyrin nanoring would be a better shape-match. The $Au_{25}(SR)_{18}$ nanocluster is essentially a three-dimensional scaffold that can be broken into three orthogonal ligand planes, each containing 8 ligands of which half are shared between planes. We performed molecular mechanics modelling of complexes ***c*-P6•$\mathbf{Au_{25}PyET_{18}^-}$** and ***c*-P8•$\mathbf{Au_{25}PyET_{18}^-}$** by docking the $\mathbf{Au_{25}PyET_{18}^-}$ nanocluster into nanorings ***c*-P6** (Figures 2 and S5) and ***c*-P8** (Figure S6), respectively. As anticipated, $\mathbf{Au_{25}PyET_{18}^-}$ is a considerably better fit to ***c*-P6**

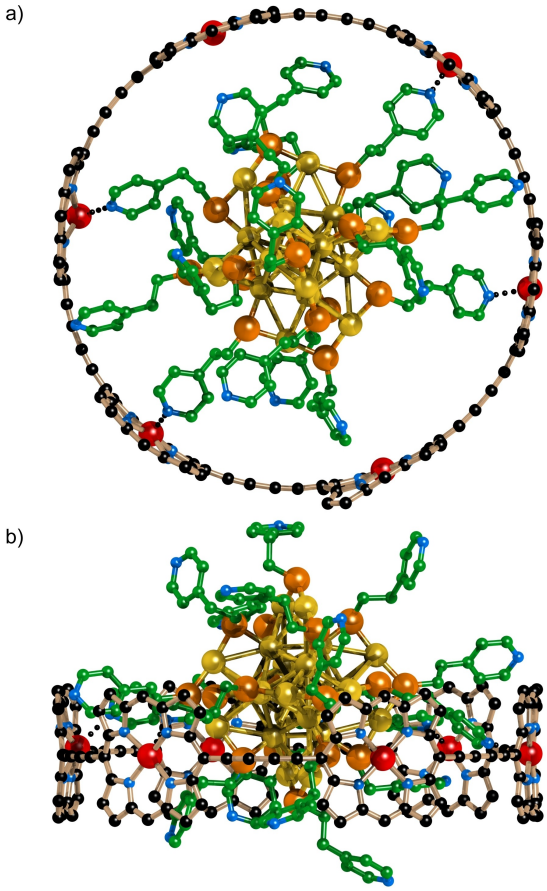

Figure 2. Top (a) and side-view (b) of a MM+ minimized model (using HyperChem) of the ***c*-P6•$\mathbf{Au_{25}PyET_{18}^-}$** host-guest complex. Atoms belonging to the core of the nanocluster ($Au_{25}S_{18}$) were frozen during the minimization. Color codes for elements: N (blue), C of the porphyrin ring (black), C of the gold nanocluster (green), S (orange), Zn (red), and Au (yellow). Aryl side groups were replaced with hydrogens to simplify the calculation.

($d_{Zn\text{-}Zn}$ = 2.56 nm) than ***c*-P8** ($d_{Zn\text{-}Zn}$ = 3.43 nm) in terms of size. However, in terms of symmetry, ***c*-P8** has a better complementarity to the ligand arrangement around the gold cluster. The nanocluster fit to ***c*-P8** could be improved by adding longer ligating chains to the cluster, however, as we aim to use the nanoring for protecting the gold cluster and as a potential energy sensitizer, we opted for $\mathbf{Au_{25}PyET_{18}^-}$ with shorter sidechains to minimize the nanocluster-to-nanoring separation.

Formation of c-PN•$Au_{25}PyET_{18}^-$ complexes

Encapsulation of the gold nanocluster $\mathbf{Au_{25}PyET_{18}^-}$ into 6-, 8-, or 10-porphyrin nanorings was tested by titrating the nanocluster into a solution of nanoring in chloroform, while monitoring the change in both absorption and fluorescence. Because of the low solubility of $\mathbf{Au_{25}PyET_{18}^-Na^+}$ in chloroform, methanol was needed to dissolve the nanocluster and as a result, a small volume-percentage of methanol was present during these experiments (between 0 and 1 %), which is expected to cause some weakening of the binding between $\mathbf{Au_{25}PyET_{18}^-}$ and the nanorings. A bathochromic shift, together with a sharpening of the lowest energy absorption band, is a distinctive feature of successful template encapsulation into the nanorings, because the template restricts the rotation of the porphyrin units around the butadiyne links and locks the nanoring in a more conjugated conformation. Gratifyingly, when $\mathbf{Au_{25}PyET_{18}^-Na^+}$ was titrated into ***c*-P6**, a well-resolved absorption band emerged with three maxima at 761, 799, and 836 nm, which is characteristic of a bound ***c*-P6** complex, and hence formation of the ***c*-P6•$Au_{25}PyET_{18}^-$** complex (Figure 3).[9,16] Likewise, the addition of $\mathbf{Au_{25}PyET_{18}^-}$ into both ***c*-P8**[17,18] and ***c*-P10**,[18] also caused the appearance of red-shifted and more structured absorption bands, implying encapsulation of the gold nanocluster. The equilibrium constant for formation of the complexes, K_f, were estimated directly from the formation titrations. Fitting of the binding curves to a 1:1 isotherm for a two-state equilibria model gave the formation constant for the three complexes, $\log_{10}K_f = 7.04 \pm 0.04$ (***c*-P6•$Au_{25}PyET_{18}^-$**), 7.49 ± 0.05 (***c*-P8•$Au_{25}PyET_{18}^-$**), and 6.69 ± 0.02 (***c*-P10•$Au_{25}PyET_{18}^-$**). Although these K_f values are high enough to achieve complete complexation between nanocluster and nanorings at the dilute concentrations used for UV/Vis titrations, they are surprisingly low compared to the binding constants measured previously for nanoring complexes of similar sizes.[9] This could be due to the ligand arrangement in $\mathbf{Au_{25}PyET_{18}^-}$, which is not ideal for binding six porphyrins equally spaced on a circle in ***c*-P6**. The presence of up to 1 % methanol in the solvent is also expected to reduce K_f. ***c*-P8** makes a better match with the ligand arrangement of the nanocluster, but the ligands in $\mathbf{Au_{25}PyET_{18}^-}$ are too short, which reduces the binding affinity for ***c*-P8** and ***c*-P10**.

Fluorescence titrations were carried out under identical conditions to the UV/Vis-NIR absorption titrations. Fluorescence originating primarily from the porphyrin nanorings was monitored during formation of the complexes

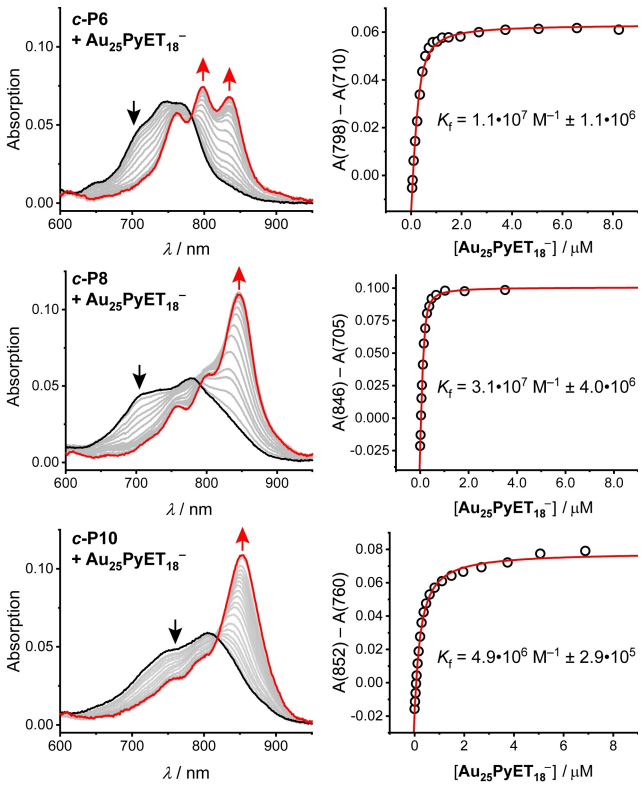

Figure 3. UV/Vis formation titrations between gold nanocluster $\mathbf{Au_{25}PyET_{18}^-}$ and nanorings ***c*-P6**, ***c*-P8**, and ***c*-P10** in $CDCl_3$ at 25 °C. Because $\mathbf{Au_{25}PyET_{18}^-}$ also absorbs between 600–950 nm, its absorption contribution has been subtracted to show the change in porphyrin nanoring absorption.

through excitation into the porphyrin Soret band (λ_{Ex} = 500 nm). When the hexa(4-(4-pyridyl)phenyl)benzene **T6** template is bound to free ***c*-P6** (Φ_F = 0.43 %) its fluorescence quantum yield drops by a factor of 4 due to rigidification of the symmetric geometry.[16] When $\mathbf{Au_{25}PyET_{18}^-}$ was added into ***c*-P6**, the porphyrin-based fluorescence intensity dropped 29-fold (97 % quenching efficiency), implying efficient energy transfer from the nanoring to the gold nanocluster or electron-hole pair separation (Figure 4). $\mathbf{Au_{25}PyET_{18}^-}$ and ***c*-P6** have almost the same HOMO–LUMO gap (ca. 1.3 eV[16,19]) so energy transfer would be energy-neutral. On the other hand, the oxidation potential of $\mathbf{Au_{25}PET_{18}^-}$ is −0.29 V[20] vs. Fc/Fc^+ and the reduction potential of ***c*-P6** is −1.29 V,[16] so photoinduced transfer of an electron from $\mathbf{Au_{25}PyET_{18}^-}$ to ***c*-P6** is expected to be favorable by about 0.30 eV. (In contrast, photoinduced electron transfer in the other direction, from ***c*-P6** to $\mathbf{Au_{25}PyET_{18}^-}$, should be unfavorable by 0.94 eV, calculated from the first reduction potential of $\mathbf{Au_{25}PET_{18}^-}$ at −1.91 V[20] and the first oxidation potential of ***c*-P6** at −0.33 V.[16]) A similar fluorescence quenching effect, due to the gold cluster acting as an excited state electron donor, has been reported in pyrene-functionalized Au_{25} clusters.[21]

The porphyrin fluorescence was partially quenched upon addition of $\mathbf{Au_{25}PyET_{18}^-}$ to ***c*-P8** (91 % quenching efficiency), and ***c*-P10** (80 % quenching efficiency), however to

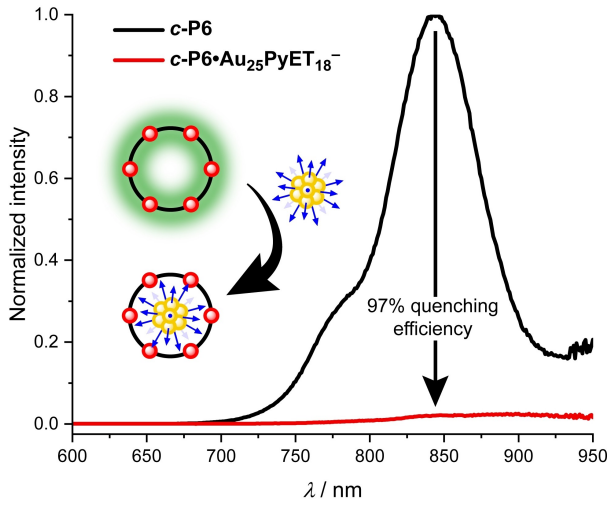

Figure 4. Fluorescence spectra of ***c*-P6** (black) and ***c*-P6•$Au_{25}PyET_{18}^-$** (red) in chloroform at 25 °C (λ_{Ex} = 500 nm).

a lesser extent than with ***c*-P6** (Figures S7–S9), implying that quenching is most efficient when the nanoring is at a short distance from the nanocluster. When pyridine was added to the complexes, ***c*-P*N*•$Au_{25}PyET_{18}^-$** (N = 6, 8, 10), fluorescence was recovered in all cases, showing that pyridine acts as a competing ligand for the zinc metal sites of the nanorings (Figure S10–13).

Negative mode mass spectrometry (MALDI-MS) confirmed the formation of a 1:1 complex, ***c*-P6•$Au_{25}PyET_{18}^-$** (Figure S15a). When ***c*-P6** was mixed with **$Au_{25}PyET_{18}^-$**, new peaks appeared in the m/z range 12,000–14,000, matching well with the calculated masses (Figure S15b). Specifically, the peaks at m/z = 13942.8 and m/z = 12602.3 can be attributed to ***c*-P6•$Au_{25}PyET_{18}^-$** and ***c*-P6•$Au_{21}PyET_{14}^-$** (formed by loss of Au_4PyET_4), respectively. Note that Au_4SR_4 (SR = thiolate) is a typical fragment of Au_{25} and other clusters in mass spectrometry.[13] In control experiments, we recorded UV/Vis spectra and mass spectra of mixtures of ***c*-P6** and **$Au_{25}PET_{18}$** (PET = 2-phenylethylthiolate) instead of **$Au_{25}PyET_{18}^-$**. Addition of the **$Au_{25}PET_{18}$** nanocluster to ***c*-P6** did not result in any shift in the UV/Vis spectrum associated with a host–guest assembly (Figure S16a). Moreover, the MALDI mass spectrum of a 1:1 mixture of **$Au_{25}PET_{18}$** and ***c*-P6** (Figure S16b), does not show the characteristic peaks in the range of m/z = 12,000–14,000 associated with the nanocluster-nanoring assembly. These findings indicate that the assembly of Au nanoclusters and ***c*-P6** to form a 1:1 complex results from the interaction between the nitrogen atoms in the protecting ligands of Au nanoclusters and ***c*-P6**, rather than solely from trapping the nanoclusters inside the nanoring.

The stability of **$Au_{25}PyET_{18}^-$** was assessed both in its pure form and after assembly of ***c*-P6•$Au_{25}PyET_{18}^-$**. This evaluation is crucial given that the poor stability in Au nanoclusters for long-term use or storage, especially in solution, is a major obstacle for this class of materials.[22] The UV/Vis spectra of a solution containing **$Au_{25}PyET_{18}^-$** in a mixture of chloroform and methanol were compared over time (in the dark at 298 K) with the same solution containing the 1:1 complex ***c*-P6•$Au_{25}PyET_{18}^-$**. As illustrated in Figure 5a, the UV/Vis spectra of **$Au_{25}PyET_{18}^-$** underwent significant changes over time, resulting in the gradual disappearance of characteristic peaks. After 18 hours, the broad band around 670 nm, due to the nanoclusters, had nearly vanished, and after 120 hours, a new absorption peak around 550 nm emerged, attributed to the surface plasmon resonance, typically observed in larger Au nanoparticles. In contrast, the UV/Vis spectra of the 1:1 assembly (Figure 5b) remained almost unchanged even after 120 h. MALDI-MS analysis corroborated these findings. Figure 5c illustrates the emergence of multiple new peaks in **$Au_{25}PyET_{18}^-$** over time. Whereas, in ***c*-P6•$Au_{25}PyET_{18}^-$** the characteristic peak of the nanocluster at m/z = 6068.7 and associated peaks of the assembly at m/z = 13941.4 and m/z = 13835.6 remain clearly observable without significant changes even after 120 hours (Figure 5d). These results demonstrate that the host, ***c*-P6**, significantly improves the stability of **$Au_{25}PyET_{18}^-$** through supramolecular encapsulation.

Following the successful formation of ***c*-P6•$Au_{25}PyET_{18}^-$**, an investigation into the excited-state energy and charge transfer between **$Au_{25}PyET_{18}^-$** and ***c*-P6** was conducted. We used time-resolved photoluminescence (PL) and electrochemical impedance spectroscopy (EIS) to examine the energy and charge transfer process. As evident from the results of Figure S17a, the average PL decay for ***c*-P6•$Au_{25}PyET_{18}^-$** is faster compared to pure ***c*-P6**, which could be due to efficient energy transfer or photoinduced electron transfer between the nanoring and gold nanocluster in the assembly. The results of EIS (Figure S17b) show that the charge transfer resistance (R_{ct}) significantly decreases to 5.63 ohms in the ***c*-P6•$Au_{25}PyET_{18}^-$**, compared to both **$Au_{25}PyET_{18}^-$** (10.08 ohms) and ***c*-P6** (32.41 ohms) under dark conditions. The decrease in resistance and enhancement in charge transfer for ***c*-P6•$Au_{25}PyET_{18}^-$** could be due to the contribution of the conjugated structure of the nanoring assembly with the Au nanocluster. Upon illumination, the EIS of ***c*-P6•$Au_{25}PyET_{18}^-$** decreased to 4.87 ohms, implying that the photo-illumination could promote photoinduced electron transfer between **$Au_{25}PyET_{18}^-$** and ***c*-P6**.[23] These results indicate that encapsulation of the Au nanocluster inside the nanoring provides an efficient charge transfer pathway.

Catalytic activity of the c-P6•$Au_{25}PyET_{18}^-$ assembly

The observation that encapsulation of **$Au_{25}PyET_{18}^-$** by ***c*-P6** can accelerate energy and/or charge transfer under light, implies that the ***c*-P6•$Au_{25}PyET_{18}^-$** assembly possesses great potential as a catalyst for both photocatalytic and photoelectrocatalytic reactions. Therefore, we investigated the efficiency of ***c*-P6•$Au_{25}PyET_{18}^-$** in photo-coupled electrocatalytic CO_2 conversion and photocatalytic singlet oxygen generation.

In the first experiment, both electrocatalytic and photocoupled electrocatalytic CO_2 reduction activities of ***c***-

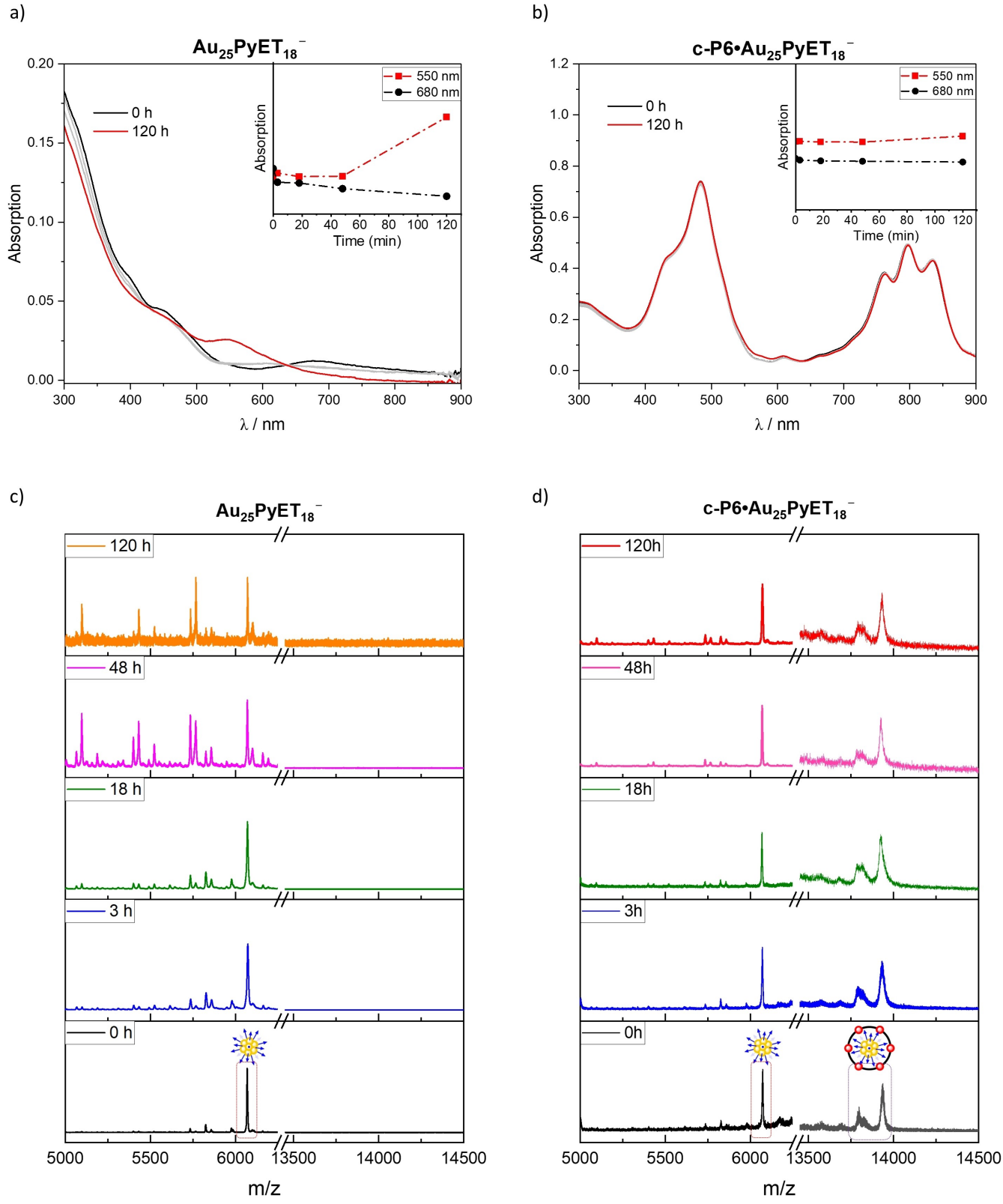

Figure 5. Time dependent UV/Vis and MALDI-MS spectra of (a, c) **$Au_{25}PyET_{18}^-$** and (b, d) ***c*-P6•$Au_{25}PyET_{18}^-$** in chloroform/methanol (99.5 : 0.5) at 25 °C. The right side of the MALDI spectra (*m/z*: 13,500–14,500) has been magnified.

P6•$Au_{25}PyET_{18}^-$ were evaluated in comparison with pristine **$Au_{25}PyET_{18}^-$** and ***c*-P6**, in a CO_2-saturated 0.5 M $KHCO_3$ electrolyte using a three-electrode-based H-cell equipped with a 300 W Xe lamp and water-cooling system (Fig-

ure S18). The linear sweep voltammograms (LSVs) demonstrate that ***c*-P6•$Au_{25}PyET_{18}^-$** exhibits higher current densities in a CO_2-saturated solution than those measured in the corresponding N_2-saturated electrolyte (Figure S19), verifying that the activity from the CO_2 reduction is predominant over the hydrogen evolution reaction. Under illumination in CO_2-saturated solution, ***c*-P6•$Au_{25}PyET_{18}^-$** exhibits a more positive onset potential and higher current density, which can reach 43 mA cm^{-2} at −1.07 V vs RHE (Figure 6a). The enhancement resulting from the use of light for the assembly is stronger than that for **$Au_{25}PyET_{18}^-$** and ***c*-P6**. These results suggest that the assembly of **$Au_{25}PyET_{18}^-$** and ***c*-P6** effectively harvests photons and rapidly transfers the excited electron from the cluster to the nanoring, thus assisting CO_2 reduction.

To better study the photo-induced electron transfer efficiency, the photocurrent response for ***c*-P6•$Au_{25}PyET_{18}^-$** in comparison with pristine **$Au_{25}PyET_{18}^-$** and ***c*-P6** at −0.67 V vs. RHE were investigated and the results are shown in Figure 6b. It is evident that the light illumination enhances the current density, especially for the assembly. ***c*-P6•$Au_{25}PyET_{18}^-$** exhibits a photocurrent response of ~1.2 mA/cm^2. This value is more than two times, and six times, higher as compared to **$Au_{25}PyET_{18}^-$** (~0.5 mA/cm^2), and ***c*-P6** (~0.2 mA/cm^2), respectively, indicating a synergic enhancement in light harvesting efficiency of the nanocluster and nanoring on formation of the assembly.

The influence of light on the Faradaic efficiency of CO (FE_{CO}), partial current density of CO (j_{CO}), and turnover frequencies (TOF) were also determined. The activity test of these structures showed exclusive generation of CO and H_2 as products, with a total FE of approximately 100 % detected by online gas chromatography (GC). This finding is in good agreement with ^{1}H NMR measurement (Figure S20), which showed no sign of organic products ($C_xH_yO_z$). We conclude that no or very little organic products are formed under these conditions. As shown in the Figure 6c, when coupled with light, the FE_{CO} of ***c*-P6•$Au_{25}PyET_{18}^-$** exceeds more than 90 % in the range between −0.47 and −0.67 V, reaching a maximum of 92.1 % at −0.67 V vs RHE, which is higher compared to dark settings (82.3 % at −0.67 V vs RHE). Notably, these values are higher than those for pure **$Au_{25}PyET_{18}^-$** (79.4 % and 79.1 % at −0.67 V vs RHE under light and dark conditions, respectively), which is also evident from the raw GC traces (see Figure S21 for exemplary GC traces). In contrast, with pure ***c*-P6**, the amount of product was negligible and not detectable below −0.87 V vs RHE.

The partial current density of CO measured under dark and light conditions for ***c*-P6•$Au_{25}PyET_{18}^-$** (Figure 6d) shows that j_{CO} could be significantly increased in a potential range from −0.47 V to −0.67 V. Interestingly, these values are almost twice as high over this potential range compared to the pure Au nanocluster. The effect of the light is more apparent with the increase of potential, so that the improvement of CO partial current density is more obvious at higher potentials. More specifically, under illumination, j_{CO} increases from 13.1 mA/cm^2 (with TOF = 3402 h^{-1}) to 19.3 mA/cm^2 (with TOF = 5013 h^{-1}) at −0.87 V for ***c*-P6•$Au_{25}PyET_{18}^-$**. This enhancement for **$Au_{25}PyET_{18}^-$** was from 7.1 mA/cm^2 (with TOF = 981 h^{-1}) to 8.7 mA/cm^2 (with TOF = 1202 h^{-1}) at −0.87 V and from 0.5 mA/cm^2 (with TOF = 60 h^{-1}) to 0.9 mA/cm^2 (with TOF = 109 h^{-1}) for ***c*-P6** at the same potential, clearly showing the efficiency of the assembly, especially under illumination.

In brief, upon light irradiation, while fixing other reaction parameters, ***c*-P6•$Au_{25}PyET_{18}^-$** showed more positive onset potentials and higher FE_{CO}, j_{CO}, and TOFs than when measured in the dark. Moreover, these values were higher than those for pure **$Au_{25}PyET_{18}^-$** and ***c*-P6**, especially under illumination. These results indicate that the assembly of **$Au_{25}PyET_{18}^-$** and ***c*-P6** can synergistically enhance electron transfer to CO_2 and improve the electrocatalytic and photoelectrocatalytic activity of Au nanoclusters, which are recognized as active catalysts for CO_2 reduction.[24] These results demonstrate some of the highest activity and selectivity at lower potentials for CO_2 conversion to CO reported for Au-based catalysts (as shown in Table S2).

A possible explanation for the higher activity in the assembly compared to the pure **$Au_{25}PyET_{18}^-$** and ***c*-P6**, especially under light illumination may be that encapsulation of the Au nanocluster by ***c*-P6** provides an efficient funneling of the excitation from ***c*-P6** to **$Au_{25}PyET_{18}^-$**, thereby further promoting CO_2 reduction upon illumination in comparison to pristine **$Au_{25}PyET_{18}^-$**.

The catalytic kinetics were examined by computing Tafel curves (Figure 6e), revealing a decrease in Tafel slopes from 356 mV dec^{-1} to 312 mV dec^{-1} for ***c*-P6•$Au_{25}PyET_{18}^-$** under illumination. These values are smaller than that of **$Au_{25}PyET_{18}^-$** (384 mV dec^{-1} under dark and 370 mV dec^{-1} under light conditions). This suggests that ***c*-P6•$Au_{25}PyET_{18}^-$** exhibits favorable CO_2 to CO kinetics, potentially owing to its high initial electron transfer efficiency during the catalytic process. The Tafel slopes are much larger than 118 mV dec^{-1}, which implies that the single electron transfer to adsorbed CO_2 ($*CO_2 + e^- \rightarrow *COO^-$) is the rate determining step.[25] Additionally, it implies that an external light field can expedite electron transfer in the assembly compared to the pristine nanocluster.

Stability is one of the most important parameters that should be considered when designing catalysts. Indeed, pristine Au nanoclusters suffer from poor stability under light irradiation.[7,26] Therefore, the photo-coupled electrocatalytic stability test for **$Au_{25}PyET_{18}^-$** and ***c*-P6•$Au_{25}PyET_{18}^-$** was performed at −0.67 V vs. RHE (Figure 6f). The stability test shows that both current density and FE_{CO} for **$Au_{25}PyET_{18}^-$** are subject to a drop from ~5.6 mA/cm^{-2} to ~3.1 mA/cm^{-2} and from ~79 % to ~73 %, respectively, after a 10-hour stability test. However, neither considerable current density drop nor FE_{CO} decrease was observed during the stability test for ***c*-P6•$Au_{25}PyET_{18}^-$**. The excitation of Au nanoclusters upon illumination may cause instability (e.g. loss of ligands) and finally aggregation and formation of nanoparticles during light illumination.[7b] The encapsulation of **$Au_{25}PyET_{18}^-$** with ***c*-P6** can protect the cluster from aggregation and prevent the formation of larger nanoparticles. This hypothesis can provide us with a strategy

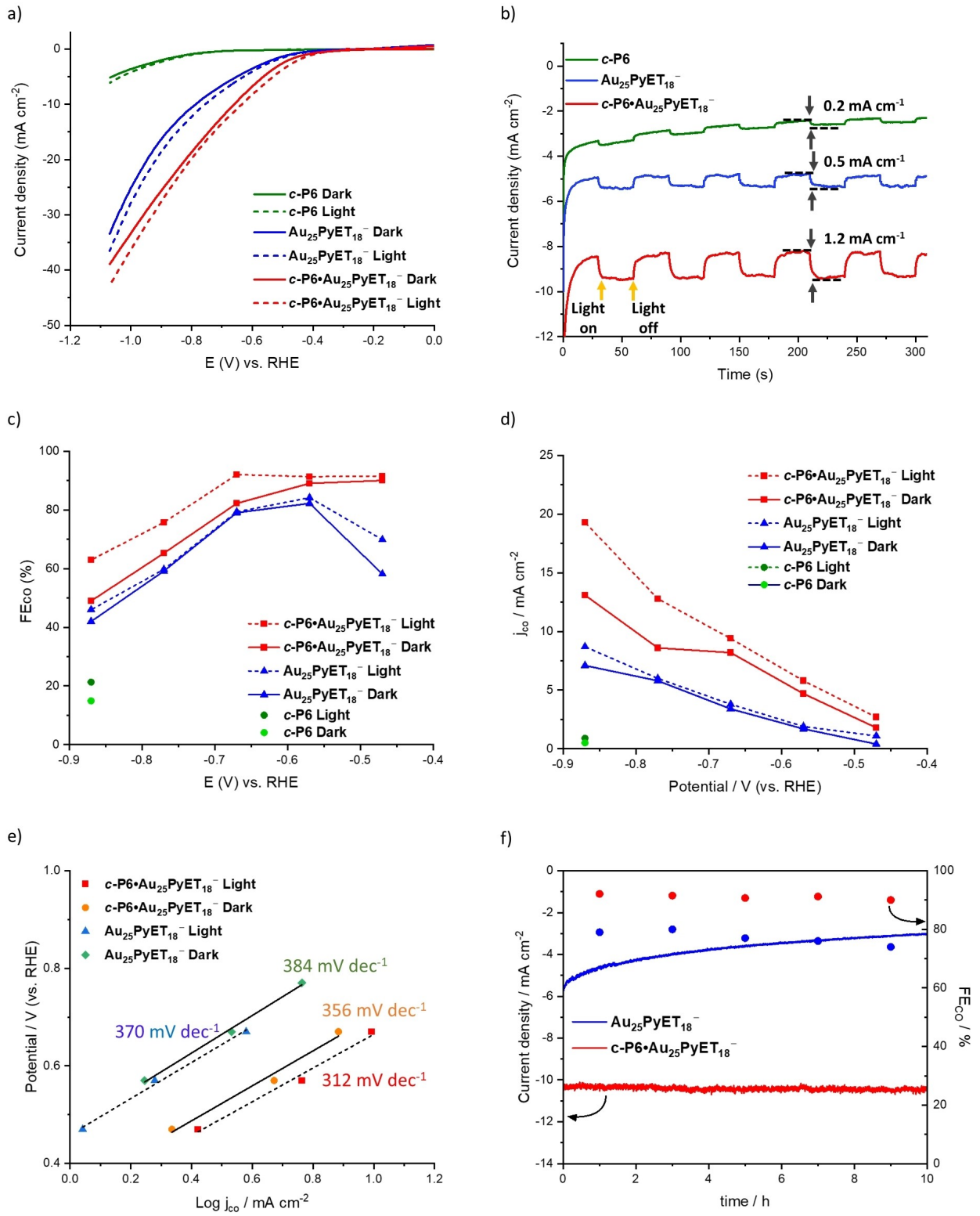

Figure 6. Electrocatalytic and photo-coupled electrocatalytic CO_2 reduction performances. a) LSV curves, b) Photocurrent response at −0.67 V vs. RHE, c) FE_{CO} and d) j_{CO} of ***c*-P6**, **$Au_{25}PyET_{18}^-$** and ***c*-P6•$Au_{25}PyET_{18}^-$** under dark and light conditions. e) Tafel plot under dark and light conditions and f) Stability test at −0.67 V vs. RHE under light illumination for **$Au_{25}PyET_{18}^-$** and ***c*-P6•$Au_{25}PyET_{18}^-$**.

to improve the stability of Au nanoclusters during photocatalytic reactions.

Singlet oxygen generation

To further investigate the efficiency of ***c*-P6•$Au_{25}PyET_{18}^-$** in a catalytic reaction under illumination, the visible light-driven $^1O_2$ evolution activity of ***c*-P6•$Au_{25}PyET_{18}^-$**, **$Au_{25}PyET_{18}^-$** and ***c*-P6** was screened using a photo-bleaching experiment with the chemical trapping probe, 1,3-diphenylisobenzofuran (DPBF), a commonly used compound for trapping $^1O_2$ in organic media.[27] Figure S22 depicts the time-dependent behavior of different catalysts under the illumination of an LED at 500 nm. The left panel captures alterations in the absorption spectra, while the right panel illustrates changes in the maximum absorbance of DPBF exclusively. Furthermore, the upper right panel shows the fit of the time-dependent model described in the Supporting Information, along with the corresponding residuals.

Our results illustrate that the absorption band of DPBF around 410 nm diminishes upon photoirradiation of ***c*-P6•$Au_{25}PyET_{18}^-$**, **$Au_{25}PyET_{18}^-$** and ***c*-P6** (Figure S23, S24). This indicates reaction of DPBF with $^1O_2$ generated upon excitation of the corresponding photosensitizer. Notably, the right panels highlight that the change in the maximum absorbance of DPBF using the ***c*-P6•$Au_{25}PyET_{18}^-$** assembly is more rapid than for pristine **$Au_{25}PyET_{18}^-$** and ***c*-P6**, suggesting a more efficient visible light-driven singlet oxygen generation with the assembly.

In order to quantify the singlet oxygen quantum yields for ***c*-P6•$Au_{25}PyET_{18}^-$**, **$Au_{25}PyET_{18}^-$** and ***c*-P6** we used Rose Bengal as secondary standard, as described in the SI. The $^1O_2$ quantum yield for ***c*-P6•$Au_{25}PyET_{18}^-$** was calculated to be 48 %, whereas the values for pristine **$Au_{25}PyET_{18}^-$** and ***c*-P6** were 18 % and 12 %, respectively. This outcome indicates that the assembly between **$Au_{25}PyET_{18}^-$** and ***c*-P6** significantly enhances its efficiency for $^1O_2$ generation.

Conclusions

In conclusion, we have investigated a host–guest system formed by binding atomically precise Au nanoclusters inside zinc porphyrin nanorings. The formation and improved stability of the assembled structure, compared to pristine nanoclusters, were confirmed through various analytical techniques. Our results reveal the significant role of the assembly between **$Au_{25}PyET_{18}^-$** and ***c*-P6** in different catalytic activities, ranging from CO_2 reduction to $^1O_2$ generation. EIS and time-resolved PL analyses demonstrated enhanced energy or electron transfer efficiency in the assembled configuration. Catalytic investigations unveiled the remarkable activity and selectivity for both CO_2 to CO conversion and singlet oxygen generation. Importantly, the assembled structure exhibited superior stability during prolonged catalytic testing, suggesting its potential for enduring applications in diverse catalytic processes. This work contributes to the understanding of host–guest interactions involving metal nanoclusters and opens avenues for designing efficient and stable nanocatalysts for various applications.

Acknowledgements

T.B. acknowledges the generous support from the Swiss National Science Foundation (grant 200020_214996) and from the University of Geneva. H.G. and H.L.A. acknowledge funding from the European Research Council (grant 885606, ARO-MAT). We thank Dr. Emmanuel Varesio and the Mass Spectrometry core facility (MZ ChemBio) for MS measurement, and Ishida Yohei for sharing the crystallographic coordinates of **$Au_{25}PyET_{18}Na$**.[11] For the purpose of Open Access, the authors have applied a CC BY public copyright license to any Author Accepted Manuscript (AAM) version arising from this publication. Open Access funding provided by Université de Genève.

Conflict of Interest

The authors declare no conflict of interest.

Data Availability Statement

The data that support the findings of this study are openly available in Zenodo at https://doi.org/10.5281/zenodo.14066646

Keywords: Au nanocluster• nanoring · host-guest chemistry · CO_2 reduction · singlet oxygen generation

[1] a) I. Chakraborty, T. Pradeep, *Chem. Rev.* **2017**, *117*, 8208–8271; b) Y. Du, H. Sheng, D. Astruc, M. Zhu, *Chem. Rev.* **2019**, *120*, 526–622; c) T. Kawawaki, A. Ebina, Y. Hosokawa, S. Ozaki, D. Suzuki, S. Hossain, Y. Negishi, *Small* **2021**, *17*, 2005328.

[2] a) T. Kawawaki, Y. Negishi, H. Kawasaki, *Nanoscale Adv.* **2020**, *2*, 17–36; b) C. Li, O. J. H. Chai, Q. Yao, Z. Liu, L. Wang, H. Wang, J. Xie, *Mater. Horiz.* **2021**, *8*, 1657–1682.

[3] J. Zhang, H.-D. Wang, Y. Zhang, Z. Li, D. Yang, D. H. Zhang, T. Tsukuda, G. Li, *J. Phys. Chem. Lett.* **2023**, *14*, 4179–4184.

[4] H. Kawasaki, S. Kumar, G. Li, C. Zeng, D. R. Kauffman, J. Yoshimoto, Y. Iwasaki, R. Jin, *Chem. Mater.* **2014**, *26*, 2777–2788.

[5] Y. Wang, Y. Lin, S. He, S. Wu, C. Yang, *J. Hazard. Mater.* **2023**, 132538.

[6] a) J. Zhao, A. Ziarati, A. Rosspeintner, T. Bürgi, *Angew. Chem. Int. Ed.* **2024**, *63*, e2023166; b) X. Cui, J. Wang, B. Liu, S. Ling, R. Long, Y. Xiong, *J. Am. Chem. Soc.* **2018**, *140*, 16514–16520.

[7] a) B. Weng, Y. Jiang, H.-G. Liao, M. B. Roeffaers, F. Lai, H. Huang, Z. Tang, *Nano Res.* **2021**, *14*, 2805–2809; b) B. Weng, K.-Q. Lu, Z. Tang, H. M. Chen, Y.-J. Xu, *Nat. Commun.* **2018**, *9*, 1543.

[8] C.-K. Yong, P. Parkinson, D. V. Kondratuk, W.-H. Chen, A. Stannard, A. Summerfield, J. K. Sprafke, M. C. O'Sullivan, P. H. Beton, H. L. Anderson, L. M. Herz, *Chem. Sci.* **2015**, *6*, 181–189.

[9] H. J. Hogben, J. K. Sprafke, M. Hoffmann, M. Pawlicki, H. L. Anderson, *J. Am. Chem. Soc.* **2011**, *133*, 20962–20969.

[10] P. S. Bols, H. L. Anderson, *Acc. Chem. Res.* **2018**, *51*, 2083–2092.

[11] Z. Huang, Y. Ishida, T. Yonezawa, *Angew. Chem. Int. Ed.* **2019**, *58*, 13411–13415.
[12] M. D. Peeks, C. E. Tait, P. Neuhaus, G. M. Fischer, M. Hoffmann, R. Haver, A. Cnossen, J. R. Harmer, C. R. Timmel, H. L. Anderson, *J. Am. Chem. Soc.* **2017**, *139*, 10461–10471.
[13] a) J. F. Parker, C. A. Fields-Zinna, R. W. Murray, *Acc. Chem. Res.* **2010**, *43*, 1289–1296; b) X. Kang, H. Chong, M. Zhu, *Nanoscale* **2018**, *10*, 10758–10834; c) Y. Cao, T. Chen, Q. Yao, J. Xie, *Acc. Chem. Res.* **2021**, *54*, 4142–4153.
[14] a) M. Zhu, C. M. Aikens, F. J. Hollander, G. C. Schatz, R. Jin, *J. Am. Chem. Soc.* **2008**, *130*, 5883–5885; b) M. W. Heaven, A. Dass, P. S. White, K. M. Holt, R. W. Murray, *J. Am. Chem. Soc.* **2008**, *130*, 3754–3755.
[15] M. Jirašek, M. Rickhaus, L. Tejerina, H. L. Anderson, *J. Am. Chem. Soc.* **2021**, *143*, 2403–2412.
[16] J. K. Sprafke, D. V. Kondratuk, M. Wykes, A. L. Thompson, M. Hoffmann, R. Drevinskas, W.-H. Chen, C. K. Yong, J. Kärnbratt, J. E. Bullock, M. Malfois, M. R. Wasiewlewski, B. Albinsson, L. M. Herz, D. Zigmantas, D. Beljonne, H. L. Anderson, *J. Am. Chem. Soc.* **2011**, *133*, 17262–17273.
[17] M. Hoffmann, C. J. Wilson, B. Odell, H. L. Anderson, *Angew. Chem. Int. Ed.* **2007**, *46*, 3122–3125.
[18] S. Liu, D. V. Kondratuk, S. A. L. Rousseaux, G. Gil-Ramírez, M. C. O'Sullivan, J. Cremers, T. D. W. Claridge, H. L. Anderson, *Angew. Chem. Int. Ed.* **2015**, *54*, 5355–5359.
[19] a) K. Kwak, V. D. Thanthirige, K. Pyo, D. Lee, G. Ramakrishna, *J. Phys. Chem. Lett.* **2017**, *8*, 4898–4905; b) M. Zhou, Y. Song, *J. Phys. Chem. Lett.* **2021**, *12*, 1514–1519.
[20] a) S. Hossain, W. Kurashige, S. Wakayama, B. Kumar, L. V. Nair, Y. Niihori, Y. Negishi, *J. Phys. Chem. C* **2016**, *120*, 25861–25869; b) S. Antonello, N. V. Perera, M. Ruzzi, J. A. Gascoń, F. Maran, *J. Am. Chem. Soc.* **2013**, *135*, 15585–15594.
[21] M. S. Devadas, K. Kwak, J.-W. Park, J.-H. Choi, C.-H. Jun, E. Sinn, G. Ramakrishna, D. Lee, *J. Phys. Chem. Lett.* **2010**, *1*, 1497–1503.
[22] a) X. Yuan, N. Goswami, I. Mathews, Y. Yu, J. J. N. R. Xie, *Nano Res.* **2015**, *8*, 3488–3495; b) W. Kurashige, Y. Negishi, *J. Clust. Sci.* **2012**, *23*, 365–374; c) W. Hou, M. Dasog, R. W. J. Scott, *Langmuir* **2009**, *25*, 12954–12961.
[23] a) D. Yang, H. Yu, T. He, S. Zuo, X. Liu, H. Yang, B. Ni, H. Li, L. Gu, D. Wang, X. Wang, *Nat. Commun.* **2019**, *10*, 3844; b) Y. Zhou, L. Zheng, D. Yang, H. Yang, Q. Lu, Q. Zhang, L. Gu, X. Wang, *Small Methods* **2021**, *5*, e2000991.
[24] X. Cai, G. Li, W. Hu, Y. J. A. C. Zhu, *ACS Catal.* **2022**, *12*, 10638–10653.
[25] D. Yang, S. Zuo, H. Yang, Y. Zhou, Q. Lu, X. Wang, *Adv. Mater.* **2022**, *34*, 2107293.
[26] Y. Deng, Z. Zhang, P. Du, X. Ning, Y. Wang, D. Zhang, J. Liu, S. Zhang, X. Lu, *Angew. Chem. Int. Ed.* **2020**, *59*, 6082–6089.
[27] F. Wilkinson, W. P. Helman, A. Ross, *J. Phys. Chem. Ref. Data* **1993**, *22*, 113–262.

Manuscript received: August 6, 2024
Accepted manuscript online: October 21, 2024
Version of record online: November 13, 2024